

Constraining the high-density behavior of nuclear symmetry energy with direct Urca processes

Olfa Boukari,^{1,*} Tuhin Malik,^{2,†} Aziz Rabhi,^{2,3,‡} and Constança Providência^{2,§}

¹*ISEPBG-Soukra, University of Carthage, Avenue de la République BP 77-1054 Amilcar, Tunisia*

²*CFisUC, Department of Physics, University of Coimbra, 3004-516 Coimbra, Portugal*

³*LR11ES23, University of Carthage, Avenue de la République BP 77-1054 Amilcar, Tunisia*

The density dependence of the symmetry energy in relativistic mean-field models with density dependent couplings is discussed in terms of the possible opening of nucleonic direct Urca processes inside neutron stars, which induce a very rapid cooling of the star. The modification of the parametrization of the isospin channel of two models, DD2 and DDME χ , keeping the same isoscalar properties is considered and the implications are discussed. Within the models discussed it is not possible the onset of nucleonic direct Urca processes in stars with a mass below $\sim 1.6 - 1.8 M_{\odot}$. The lowest masses that allow direct Urca processes are associated to a slope of the symmetry energy ~ 60 MeV and a symmetry energy incompressibility close to zero. It is shown that the parametrization of the isospin channel proposed destroys the correlation between symmetry energy slope and incompressibility previously identified in several works.

I. INTRODUCTION

In the past decade, multi-messenger astronomy has made significant progress, particularly with the recent detection of gravitational waves (GW) by the LIGO and Virgo Collaboration (LVC). Notably, they detected GW originating from two distinct binary neutron star (BNS) mergers. The first event, known as GW170817 [1–3], involved a BNS merger with a total mass of $2.7M_{\odot}$ and mass components ranging between $1.17M_{\odot}$ and $1.6M_{\odot}$. Similarly, the subsequent detection of the GW190425 merger, as detailed in reference [4], further expanded our knowledge. This event featured a total mass of $3.4^{+0.3}_{-0.1}M_{\odot}$, with mass components spanning from $1.12M_{\odot}$ to $2.52M_{\odot}$. These observations provide valuable insights into high-density stellar matter [5–7], and offer new constraints for understanding the Equation of State (EoS) of stellar matter [8–11].

The ambitious goal of the astrophysics community is to combine these multi-messenger results to constrain the EoS of neutron stars (NSs) [5–7, 12–16], and infer the NS composition. The nuclear symmetry energy constitutes an essential ingredient to explore the macroscopic properties of NSs, and should satisfy theoretical constraints such as those obtained from chiral effective field theory (chEFT) calculations for pure neutron matter [17]. It should also be consistent with experimental and observational data.

Thanks to the considerable efforts deployed in astrophysics and nuclear physics over the last two decades, significant progress has been made in determining the symmetry energy $E_{\text{sym}}(\rho_B)$, in particular around and below the saturation density of nuclear matter ρ_0 . The

symmetry energy $E_{\text{sym}}(\rho_B)$ above saturation density and a possible hadron-quark phase transition are among the most uncertain parts of the EoS of dense neutron rich matter [18–21]. A precise determination of the behavior of $E_{\text{sym}}(\rho_B)$ at densities beyond saturation is essential. To probe the symmetry energy in this density range, data obtained from observations of NSs have revealed to be particularly useful compared with terrestrial experiments. Since the detection of GW170817, astrophysical data have stimulated many interesting studies of the symmetry energy. Recently Bao-Jun Cai et al. [22] have studied the behaviour of the nuclear symmetry energy at $2 - 3\rho_0$ on the basis of its slope L , its curvature K_{sym} and its skewness Q_{sym} at saturation ρ_0 . This investigation was achieved by developing the function $E_{\text{sym}}(\rho_B)$ in terms of a suitable auxiliary function, allowing an accurate prediction at high densities of the symmetry energy.

Several attempts have been made to obtain the EOS of supernuclear matter in NSs from different models. In particular, by adopting density-dependent DD models such as DDRMF, DD-MEX [23], DD-LZ1 [24], massive NSs with masses around $2.33 - 2.48 M_{\odot}$ could be generated. The DD models do not include mesonic nonlinear mixing or self-interaction terms. Instead, a density dependence of the nucleon-meson couplings is introduced, which takes into account the effects of the nuclear medium on the couplings, as predicted, for example, by relativistic Dirac-Brueckner-Hartree-Fock calculations [25]. However, DD models are generally characterized by an isovector coupling Γ_{ρ} which tends to zero at higher densities. This has the consequence of softening the symmetry energy at high densities, allowing large neutron densities, and therefore these models do not predict nucleonic neutrino emission processes inside the NS that are responsible for the fast cooling of the NS, i.e. the nucleon direct Urca (DU) processes [26, 27]. In order to induce the DU processes in 1.6 to $1.8 M_{\odot}$ stars, as predicted in [28], the authors in [27, 29] have included hyperons in the star. This results in a softer EoS, which

* olfa.boukari@isepbg.ucar.tn

† tm@uc.pt

‡ rabhi@fis.uc.pt

§ cp@uc.pt

makes predicting stars with masses around or above $2M_\odot$ difficult.

Bayesian inference studies have supported the possible existence of NSs with 2.50 - $2.60M_\odot$ under the constraints of NS properties of $1.4M_\odot$ [30]. This methodology based on microscopic models offers as a major advantage, the possibility, once the inference is complete, of discussing the composition of nuclear matter properties through the EOS and the symmetry energy at high densities [31–33]. The knowledge of the symmetric nuclear matter EOS has proved to be indispensable for studying the β equilibrium condition [32, 34–36]. In this context, the authors of [33] have recently developed a Bayesian inference approach, in the framework of a density dependent model, in order to determine how the GW and NICER data constrain the high-density symmetry energy values. They have confirmed that these type of models do not allow the nucleon DU processes inside NSs. This is a characteristic of all density dependent models that describe the nucleon- ρ meson coupling as an exponential decreasing function with density. However, NS cooling curves seem to indicate that these kind of processes should be possible inside NSs with a mass $\gtrsim 1.6M_\odot$ [28]. In order to adapt these DD models at high densities, modifications have recently been introduced by Malik et al. (described in Ref. [37]) which predict nucleon DU processes inside NS. The proposed modified DD models allow to control the slope L over a large range of densities both at high and low densities. For a different parametrization of the ρ -meson coupling see also [38].

In the following we propose a set of DD models, that satisfy the set of constraints on the symmetry energy proposed in several studies [37, 39], as well as constraints from the neutron matter calculation within a chEFT approach [17], which predict the onset of DU cooling processes inside the NS. In the following, we will refer as M_{DU} the minimum NS mass where nucleon DU processes are allowed to occur. We will also discuss how some constraints on the properties of symmetry energy, as delineated in [37, 39, 40], are satisfied. In particular, considering the analysis of recent NS observations, the authors of [39] have obtained at saturation density for the symmetry energy slope $L \approx 57.7 \pm 19$ MeV, the curvature $K_{sym} \approx -107 \pm 88$ MeV, and at twice the saturation density the symmetry energy $E_{sym}(2\rho_0) \approx 51 \pm 13$ MeV, all determined at a confidence level of 68%. These values are consistent with previous values obtained from other analyses based on experimental data, ab-initio calculations and NS observations, such as [40–42]. We also consider the constraints found in [37], based on the strong correlation between the symmetry energy slope at $\rho = 2.5\rho_0$ and the DU mass M_{DU} . From this correlation it was found that the symmetry energy slope range at $2.5\rho_0$ should be in the interval $L(2.5\rho_0) \approx 54 - 48$ MeV to predict DU processes occurring inside stars with a mass $M_{DU} \gtrsim 1.6 - 1.8M_\odot$.

The present study is organized as follows. In Sec. II we review the formalism used in the analysis. In Sec. III

we discuss the properties of a set of DD models, based on the DD2 [43] and DDMEX [44] models, which predict the occurrence of nucleon DU processes within NS by modifying the parameterization of the isovector channel, keeping the same isoscalar description and the symmetry energy at saturation. In Sec. IV, we generalize our study and apply a Bayesian inference approach to study the complete isovector channel, also modifying the symmetry energy at saturation and identifying possible correlations. Finally, some conclusions are drawn in Sec. V.

II. MODELS

In this section, we review the description of nuclear matter EoS with relativistic mean-field (RMF) models with density dependent couplings, and the characterization of the density dependence of the symmetry energy through its expansion at the saturation density.

A. Field Theoretical Models with DDRMF Lagrangian

In order to study the symmetry energy at high density, we will consider RMF models with density dependent baryon-meson couplings that avoid self-interacting and mixed terms between mesons and which we designate by DD models. Within this approach, we start from a Lorentz-covariant Lagrangian density which describes baryons interacting with mesons. It is assumed the minimal coupling between the baryons and the mesons.

In the DD model, the nucleons interact with each other by exchanging scalar-isoscalar (σ), vector-isoscalar (ω^μ), and vector-isovector ($\vec{\rho}^\mu$) mesons. The DDRH Lagrangian density can be written as:

$$\begin{aligned} \mathcal{L}_{DD} = & \sum_{i=p, n} \bar{\psi}_i \left[\gamma^\mu \left(i\partial_\mu - \Gamma_\omega(\rho_B)\omega_\mu - \frac{\Gamma_\rho(\rho_B)}{2} \vec{\tau} \cdot \vec{\rho}_\mu \right) \right. \\ & - (M - \Gamma_\sigma(\rho_B)\sigma) \left. \right] \psi_i + \frac{1}{2} (\partial^\mu \sigma \partial_\mu \sigma - m_\sigma^2 \sigma^2) \\ & + \frac{1}{2} m_\omega^2 \omega_\mu \omega^\mu - \frac{1}{4} \Omega^{\mu\nu} \Omega_{\mu\nu} \\ & + \frac{1}{2} m_\rho^2 \vec{\rho}_\mu \cdot \vec{\rho}^\mu - \frac{1}{4} \mathbf{B}_{\mu\nu} \cdot \mathbf{B}^{\mu\nu}, \end{aligned} \quad (1)$$

where ψ_i represents the Dirac spinor of the nucleons, M is the nucleon mass. $\Omega_{\mu\nu}$ and $B_{\mu\nu}$ are the vector meson field tensors, γ^μ and $\vec{\tau}$ are the Dirac and the Pauli matrices, respectively. The $\Gamma_\sigma(\rho_B)$, $\Gamma_\omega(\rho_B)$ and $\Gamma_\rho(\rho_B)$ are the coupling constants of the nucleons to the meson fields σ , ω , and ρ respectively, with a corresponding meson masses are m_σ , m_ω and m_ρ .

We focus on the parameterizations of DDRMF that depend on the vector density. The nucleon-meson density-dependent coupling parameters are written in the form:

$$\Gamma_j(\rho_B) = \Gamma_j(\rho_0) h_M(x), \quad x = \rho_B/\rho_0, \quad j = \sigma, \omega, \rho \quad (2)$$

where ρ_0 is the saturation density of symmetric nuclear matter. In the present study, we consider the parameterizations DD2 [45] and DDMEX [23]. For these two parameterizations, the coupling constants of the σ and ω mesons to the nucleons are given in terms of the functions h_j [45],

$$h_j(x) = a_j \frac{1 + b_j(x + d_j)^2}{1 + c_j(x + d_j)^2}, \quad (3)$$

with $x = \rho_B/\rho_0$ and ρ_B the baryonic density. The parameters $a_j, b_j, c_j,$ and d_j are defined in [45] for DD2 and [23] for DDMEX. In the DD2 and DDMEX models, the nucleon DU processes do not occur in the NS interior because the ρ_{DU} density is greater than the central density of the most massive star, ρ_c . In order to overcome this property in [37] a generalization of the isovector channel ρ -meson coupling was proposed, including a new parameter y which controls the high-density behaviour. This parametrization will be considered in the present study:

$$h_\rho(x) = y \exp[-a_\rho(x - 1)] + (1 - y), \quad 0 < y \leq 1. \quad (4)$$

From the Lagrangian density, we obtain the following meson field equations in the mean-field approximation

$$\begin{aligned} m_\sigma^2 \sigma &= \Gamma_\sigma(\rho_B) \rho_s = \Gamma_\sigma(\rho_B) \langle \bar{\psi} \psi \rangle, \\ m_\omega^2 \omega &= \Gamma_\omega(\rho_B) \rho_B = \Gamma_\omega(\rho_B) \langle \psi^\dagger \psi \rangle, \\ m_\rho^2 \rho &= \frac{\Gamma_\rho(\rho_B)}{2} \rho_3 = \frac{\Gamma_\rho(\rho_B)}{2} \langle \psi^\dagger \tau_3 \psi \rangle, \end{aligned} \quad (5)$$

where ρ_s is the scalar density, and $\rho_3 = \rho_p - \rho_n$ with ρ_p and ρ_n , respectively, the proton and the neutron densities. The Dirac equations for the nucleons are given by

$$\begin{aligned} \left[i\gamma^\mu \partial_\mu - \gamma^0 \left(\Gamma_\omega(\rho_B) \omega + \frac{\Gamma_\rho(\rho_B)}{2} \rho \tau_3 + \Sigma_0^R(\rho_B) \right) \right. \\ \left. - M_B^* \right] \psi_B = 0, \end{aligned} \quad (6)$$

where ω and ρ define the time components of ω^μ and of the third component of $\vec{\rho}^\mu$, the nucleon isospin third components take the values $\tau_3 = 1$ and $\tau_3 = -1$ for protons and neutrons, respectively, the effective mass of nucleons is given in terms of the scalar meson σ

$$M_B^* = M - \Gamma_\sigma(\rho_B) \sigma. \quad (7)$$

and the rearrangement term Σ_0^R , due to the density dependence of coupling constants [45–47], is given by

$$\Sigma_0^R(\rho_B) = \frac{\partial \Gamma_\omega(\rho_B)}{\partial \rho_B} \omega \rho_B + \frac{1}{2} \frac{\partial \Gamma_\rho(\rho_B)}{\partial \rho_B} \rho \rho_3 - \frac{\partial \Gamma_\sigma(\rho_B)}{\partial \rho_B} \sigma \rho_s. \quad (8)$$

From the energy-momentum tensor in a uniform system, the energy density, \mathcal{E} , and the pressure, P , of infinite nuclear matter can be obtained, respectively, as

$$\mathcal{E} = \frac{1}{2} m_\sigma^2 \sigma^2 + \frac{1}{2} m_\omega^2 \omega^2 + \frac{1}{2} m_\rho^2 \rho^2$$

$$+ \sum_{i=p,n} \frac{\gamma}{2\pi^2} \int_0^{k_{F_i}} k^2 \sqrt{k^2 + M_i^{*2}} dk, \quad (9)$$

$$\begin{aligned} P &= \rho_B \Sigma_R(\rho_B) - \frac{1}{2} m_\sigma^2 \sigma^2 + \frac{1}{2} m_\omega^2 \omega^2 + \frac{1}{2} m_\rho^2 \rho^2 \\ &+ \sum_{i=p,n} \frac{\gamma}{6\pi^2} \int_0^{k_{F_i}} \frac{k^4 dk}{\sqrt{k^2 + M_i^{*2}}}, \end{aligned} \quad (10)$$

where $\gamma = 2$ is the spin degeneracy factor, and k_{F_i} is the Fermi momentum of nucleon i . The binding energy per nucleon is defined by

$$\frac{E_b}{A} = \frac{\mathcal{E}}{\rho_B} - M. \quad (11)$$

B. Nuclear symmetry energy

For nuclear matter consisting of protons and neutrons at the density ρ_B with the isospin asymmetry parameter $t = (\rho_n - \rho_p)/\rho_B$, the energy per baryon(nucleon) $E = \frac{\mathcal{E}}{\rho_B}$, can be expanded with respect to t and ρ_B :

$$E(\rho_B, \delta) \simeq E_{SNM}(\rho_B) + E_{sym}(\rho_B) t^2 + \mathcal{O}(t^4), \quad (12)$$

where $E_{SNM}(\rho_B)$ is the energy per particle of symmetric nuclear matter and the symmetry energy $E_{sym}(\rho_B)$ quantifies the energy needed to make nuclear matter more neutron rich. Assuming the charge symmetry of the nuclear forces the symmetry energy can be identified as a quadratic term in t of the energy per particle:

$$E_{sym}(\rho_B) = \frac{1}{2} \frac{\partial^2 E}{\partial t^2} \Big|_{t=0}. \quad (13)$$

To study the density dependence in a range of densities below the quark-hadron phase transition, it is common to characterize the density dependence of the SNM EOS $E_0(\rho_B)$ and the symmetry energy $E_{sym}(\rho_B)$ around the saturation density ρ_0 in terms of the parameters of the Taylor series. In the following, we consider terms until third order on the variable $x = \frac{\rho_B - \rho_0}{3\rho_0}$,

$$E_0(\rho_B) = E_0(\rho_0) + \frac{K_0}{2} x^2 + \frac{Q_0}{6} x^3, \quad (14)$$

$$\begin{aligned} E_{sym}(\rho_B) &= E_{sym}(\rho_0) + L_0 x + \frac{K_{sym,0}}{2} x^2 \\ &+ \frac{Q_{sym,0}}{6} x^3, \end{aligned} \quad (15)$$

$E_0(\rho_B) \equiv E_{SNM}(\rho_B)$ is the energy per nucleon for symmetric nuclear matter (SNM). The incompressibility coefficient K_0 and the the skewness Q_0 are, respectively,

defined by:

$$\begin{aligned} K_0 &= 9\rho_0^2 \frac{\partial^2 E}{\partial \rho_B^2} \Big|_{\rho_B=\rho_0} = 9 \left[\frac{dP_0}{d\rho_B} \right]_{\rho_B=\rho_0} \\ Q_0 &= 27\rho_0^3 \frac{\partial^3 E}{\partial \rho_B^3} \Big|_{\rho_B=\rho_0} \end{aligned} \quad (16)$$

with P_0 the SNM pressure. $E_{\text{sym}}(\rho_0)$ is the symmetry energy at saturation and the quantities L_0 , K_{sym} and Q_{sym} are its slope, curvature and skewness respectively, at saturation:

$$\begin{aligned} L_0 &= 3\rho_0 \frac{\partial E_{\text{sym}}(\rho_B)}{\partial \rho_B} \Big|_{\rho_B=\rho_0}, \\ K_{\text{sym},0} &= 9\rho_0^2 \frac{\partial^2 E_{\text{sym}}(\rho_B)}{\partial \rho_B^2} \Big|_{\rho_B=\rho_0} \\ Q_{\text{sym},0} &= 27\rho_0^3 \frac{\partial^3 E_{\text{sym}}(\rho_B)}{\partial \rho_B^3} \Big|_{\rho_B=\rho_0}. \end{aligned}$$

This is considered to be a good approximation even for small proton fraction y_p [48]. These parameters characterize the density dependence of nuclear symmetry energy around normal nuclear matter density and thus provide important information on the behavior of nuclear symmetry energy at both high and low densities. Also, the curvature parameter $K_{\text{sym},0}$ would be a significant measurement which distinguishes the different parametrizations. The shift of the incompressibility with asymmetry, is given by

$$K_{\text{asy},0} = K_{\text{sym},0} - 6L_0 - \frac{Q_0}{K_0} L_0 \approx K_{\text{sym},0} - 6L_0. \quad (17)$$

This value can be correlated to experimental observations of the giant monopole resonance (GMR) of neutron-rich nuclei [49] such as on even- A Sn isotopes with a value of $K_{\text{asy},0} = -550 \pm 100$ MeV, see discussion [50–52].

III. RESULTS AND DISCUSSION

The parameterisation of the ρ meson coupling proposed in Eq. (4) allows us to obtain a set of modified DD models consistent with both low and high density constraints. We obtain for a given symmetry energy at saturation density a range of different allowed isovector properties, in particular the symmetry energy slope L_0 and its curvature $K_{\text{sym},0}$, for the same isoscalar properties i.e incompressibility, binding energy and effective mass of the baryons as shown in Table I.

The proton fraction and other NS characteristics which are sensitive to the high density behavior of the symmetry energy are used to constrain the new parameter, y , in Eq. (4). In particular, the onset of the nucleon DU processes as discussed in [28] is an observation that constrains y , see [37].

We build a set of EOS based on the modified DD2 and DDMEX models that essentially satisfy neutron matter chiral effective field theory (chEFT) [17, 53] constraints within 2σ , as shown in Fig. 1 top panels, and verify the constraints on the symmetry energy at saturation density referred in the Introduction [37, 39, 41, 42]: a slope of nuclear symmetry energy at saturation density ρ_0 satisfying $L_0 \approx 57.7 \pm 19$ MeV at 68% confidence level and a symmetry energy at twice ρ_0 , $E_{\text{sym}}(2\rho_0) \approx 51 \pm 13$ MeV at 68% confidence level [39];

the symmetry energy and respective slope satisfying $E_{\text{sym}}(\rho_0) = (31.7 \pm 3.2)$ MeV and $L_0 = (58.7 \pm 28.1)$ MeV [40]; the slope L for a density $\approx 2.5\rho_0$ taking a value in the range 48 – 54 MeV for the nucleon DU processes to occur inside neutron stars [37].

In order to constraint the high density behavior of the symmetry energy, the parameters (y, a_ρ) were chosen such that a given M_{DU} is obtained, i.e. 1.6, 1.8, 2.0 M_\odot . Acceptable models should also satisfy the low density constraints imposed by chEFT neutron matter calculations. In Table II, some symmetric nuclear matter properties calculated at saturation density and at $2.5\rho_0$ are given for all proposed EOS. As referred before, by construction the two families of models DD2 and DDMEX have the symmetry energy at saturation $E_{\text{sym},0}$ of the original DD2 and DDMEX, given in Table I.

By analyzing Table II, it is seen that L_0 is correlated (anti-correlated) with y (a_ρ) while $L(2.5\rho_0)$ are anti-correlated (correlated) with y (a_ρ): The combined effect of the two parameters is to increase the slope of L at high densities, preventing the symmetry energy from softening. On the other hand, $K_{\text{sym},0}$ is correlated with a_ρ and anti-correlated with y : it increases when a_ρ increases and remains negative for DD2, while it can reach positive values for DDMEX. Recently, positive values for $K_{\text{sym},0}$ have been obtained in [54] in an attempt to simultaneously describe the results of PREX2 [55] and CREX [56] within a model that included the δ -meson. However, previous analysis seem to prefer negative values: in [39], the authors predict $K_{\text{sym},0} \equiv -107 \pm 88$ MeV at 68% confidence level, considering a large set observational data, a value consistent with other analyses that also considered experimental data -100 ± 100 MeV [57] and -112 ± 71 MeV [58].

In general, the effect of including the parameter y is to increase the symmetry energy slope L_0 at saturation. However, an adequate choice of both parameters (y, a_ρ) also allows to fix L_0 with a value smaller than the one of DD2, but with a much larger value of $K_{\text{sym},0}$. For the DDMEX family we have only obtained EOS with $L_0 > 49$ MeV, the value that characterizes DDMEX.

In the Fig. 1 (top panels), the pure neutron matter (PNM) chEFT EOS from [17] is included considering 1σ (dark gray) and 2σ (light gray), as well as the PNM EOS of the DD modified models for M_{DU} equal to 1.6, 1.8 and 2.0 M_\odot , the DD2 family in the left panel and the DDMEX in the right one. The constraints derived for PNM exclude DU processes inside stars with a

mass $\lesssim 1.6 M_\odot$ at 2σ . According to [28], the NS cooling curves seem to indicate that $M_{\text{DU}} \sim 1.6 - 1.8 M_\odot$. Within the DDMEX family we are not able to go below $M_{\text{DU}} = 1.8 M_\odot$ and simultaneously satisfy chEFT constraints. It is seen that within the two families and the parametrization defined in Eq. (4) for the ρ -meson coupling, the chEFT constraints of [34] are only satisfied in the complete density range within the 2σ interval. Introducing the y contribution makes the symmetry energy harder above saturation density, as expected since this term does not allow the ρ -meson coupling to converge to zero, see the middle panels. The bottom panels show the symmetry energy slope as a function of the density and the effect of the y parameter is easily identified giving rise to a kind of plateau before a soft decrease occurs at the larger densities.

TABLE I. The properties of symmetric nuclear matter at saturation density for the models under study: the nuclear saturation density ρ_0 , the binding energy per particle B/A , the incompressibility K_0 , the skewness coefficient Q_0 , the symmetry energy $E_{\text{sym},0}$, the slope of the symmetry energy L_0 , and the effective nucleon mass M^* . All quantities are in MeV, except ρ_0 which is in fm^{-3} , and the effective nucleon mass is normalized to the nucleon mass.

Model	ρ_0	B/A	K_0	$E_{\text{sym},0}$	M^*/M	Q_0
DD2 Family	0.15	-16.03	243	30.8	0.55	169
DDMEX Family	0.15	-16.09	267	32.3	0.55	877

TABLE II. The symmetric nuclear matter properties at saturation density for the models under study: The slope of the symmetry energy L_0 and the curvature $K_{\text{sym},0}$ and $K_{\text{asy},0}$ at saturation density, the slope of the symmetry energy L at 2.5 saturation density for the models under study for a set of (a_ρ, y) .

Model	a_ρ	y	L (MeV)			
			L_0	$L(2.5\rho_0)$	$K_{\text{sym},0}$	$K_{\text{asy},0}$
DD2 family:						
DD2	0.5	1.0	55.12	30.27	-93.21	-415.93
DD2-2a	0.8	0.51	63.85	43.16	-52.18	-429.84
DD2-2b	1.0	0.47	59.38	45.53	-34.93	-386.78
DD2-2c	1.2	0.45	53.59	46.60	-9.62	-328.576
DD2-1.8a	1.05	0.4	62.18	48.60	-28.76	-398.01
DD2-1.8b	1.2	0.38	59.55	50.05	-13.45	-367.96
DD2-1.6a	1.25	0.29	66.33	55.45	-9.636	-405.16
DD2-1.6b	1.3	0.3	64.50	54.95	-5.078	-406.86
DDMEX family:						
DDMEX	0.6	1.0	49.66	29.87	-71.57	-369.17
DDMEX-2a	1.0	0.42	65.41	48.27	-8.08	-410
DDMEX-2b	1.1	0.4	63.85	49.60	-8.09	-390.84
DDMEX-2c	1.2	0.41	59.75	49.34	3.92	-354.25
DDMEX-1.8a	1.2	0.33	67.31	54.18	1.92	-401.68
DDMEX-1.8b	1.3	0.3	67.80	56.38	11.1	-395.4
DDMEX-1.6	1.3	0.27	70.86	58.53	10.78	-411.88

By varying (y, a_ρ) it is possible to increase the slope of the symmetry energy at $2.5\rho_0$ with respect to the original models, DD2 and DDMEX: $L(2.5\rho_0)$ varies in the range [43,55] MeV for DD2 family and [48,58] MeV for DDMEX family. This intervals are reasonably compatible with $L(2.5\rho_0) \equiv 48 - 54$ MeV, taking into account that they have been deduced from the strong correlation existing between L and M_{DU} [37],

$$\frac{L}{\text{MeV}} = \frac{-31.224}{\text{MeV}} \frac{M_{\text{DU}}}{M_\odot} + \frac{104.339}{\text{MeV}} \quad (18)$$

with a Pearson coefficient of 0.9.

DDMEX model presents a softer EoS with a lower slope $L_0 = 49.7$ MeV that satisfies the 1σ constraint as shown in Fig.1. We notice, the higher the slope the stiffer is the pressure. The DDMEX-1.6 model has $L_0 = 70.9$ MeV and misses the chiral EFT above 0.13fm^{-3} .

In Fig. 2, $K_{\text{sym},0}$ is plotted versus L_0 changing the parameter y between 0 and 1, and considering several values for the a_ρ parameter. A negative correlation between L_0 and $K_{\text{sym},0}$ is obtained when a_ρ takes the original values of models DD2[43] and DDMEX [44]. A similar correlation was obtained in [59–61], where it was shown that the coefficients L_0 and $K_{\text{sym},0}$ taken at saturation density for a large set of RMF and Skyrme force models present a linear anti-correlation between them. However, for the modified EOS with a larger parameter a_ρ , the L_0 - $K_{\text{sym},0}$ variation is not monotonic, showing that the L_0 - $K_{\text{sym},0}$ correlation is washed out for sufficiently large values of the parameter a_ρ .

A. Direct Urca process with modified DD models

In this section, we investigate the opening density of the direct DU process for the modified density-dependent model families. The nucleonic DU processes [62] by neutrino emission are described by the equations :

$$n \rightarrow p + e^- + \bar{\nu}_e, \quad \text{and} \quad p + e^- \rightarrow n + \nu_e. \quad (19)$$

This process is considered to be the most efficient NS cooling mechanism. It is only triggered if there is conservation of momentum, i.e. $p_{Fn} \leq p_{Fp} + p_{Fe}$, where p_{Fi} is the Fermi momentum of the particle species i .

Therefore, the proton fraction needs to equal or exceed a minimum proton fraction y_p^{min} [63], to allow the DU process to operate:

$$y_p^{\text{min}} = \frac{1}{1 + \left(1 + x_e^{1/3}\right)^3}, \quad (20)$$

with $x_e = \rho_e / (\rho_e + \rho_\mu)$, and ρ_e and ρ_μ the electron and muon densities. In the following, ρ_{DU} denotes the baryon density at which the DU process starts to operate and M_{DU} is the mass of the star with a central density equal to ρ_{DU} .

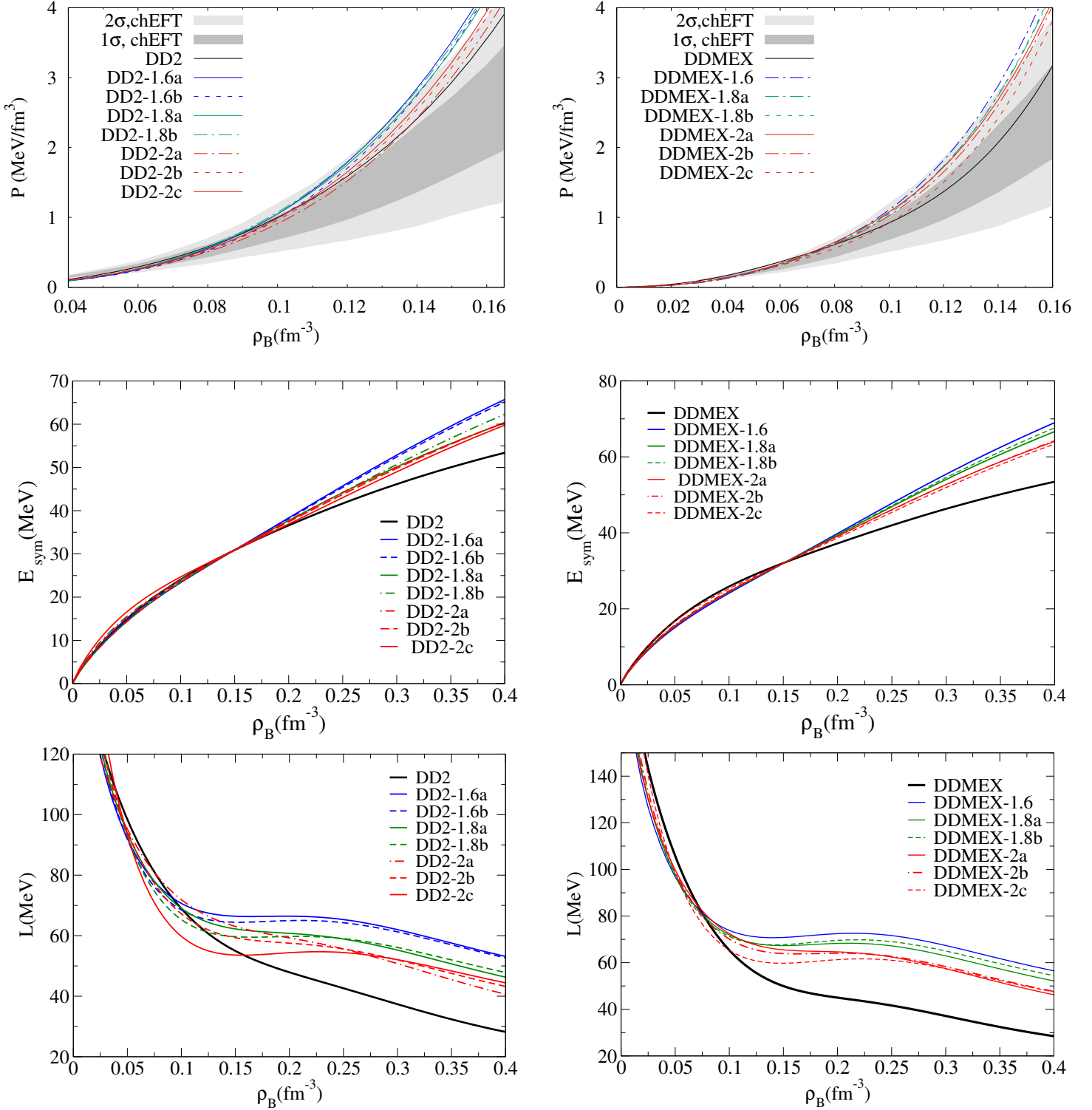


FIG. 1. (Color online) Upper panels show the pure neutron matter pressure as a function of the baryonic density for DD2 (left) and DDMEX (right) families under consideration varying (a_ρ, y) to obtain a given M_{DU} i.e. 1.6, 1.8, 2.0 M_\odot and including the 1σ and 2σ bands from chiral effective field theoretical calculations [17]. Middle panels reveal the symmetry energy and in the bottom its slope as function of the baryon density for DD2 (left) and DDMEX (right) families.

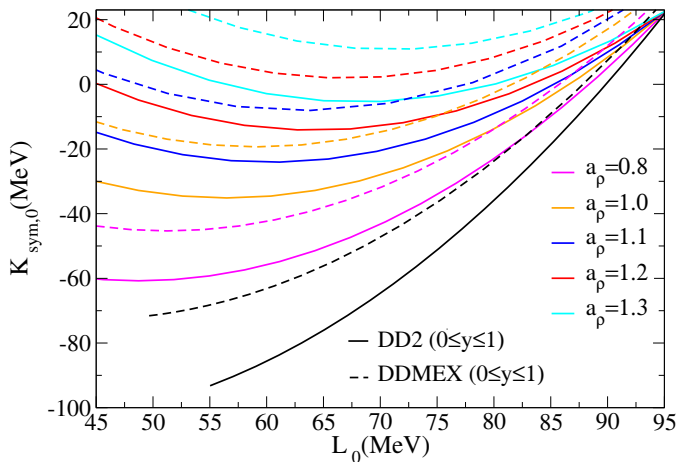


FIG. 2. $K_{sym,0}$ versus L_0 . Original DD2 (black solid line) and DDMEX (black dashed line) varying y , modified DD2 (colored solid line) and DDMEX (colored dashed line) using different values of the parameter a_ρ and varying y .

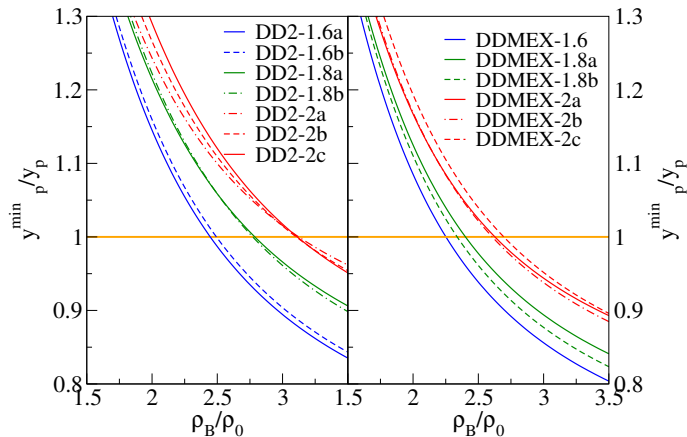


FIG. 3. (Color online) The DU onset for a given M_{DU} , i.e. 1.6, 1.8, 2.0 M_\odot (blue, green, red), for the DD2 family (left) and the DDMEX family (right).

In previous studies [59, 64], the authors investigated how the symmetry energy in various non-linear RMF models affects the DU process, emphasizing its connection to the density dependence of symmetry energy. They discovered that this dependence notably influences this process. In cases like DD2 and DDMEX models, nucleonic DU processes are prohibited, as in most conventional DD models. However, fast cooling can still occur with hyperon onset. In such cases, hyperonic DU processes, involving hyperon decay into other hyperons or nucleons with neutrino emission, begin just above hyperon onset densities [26].

To explore the impact of the density dependence of the symmetry energy slope L on the DU processes, we depict in Fig. 3 the onset density of nuclear DU processes

the DD modified models discussed in Table II to illustrate the relationship between baryon density and the ratio of proton fractions, y_p^{\min}/y_p , where y_p is the β -equilibrium proton fraction. The onset of the DU process occurs when this ratio, y_p^{\min}/y_p , is less or equal to 1. By analyzing the onset of the DU process at ρ_{DU} , we can classify three sets of EOS based on similar densities: $\sim 2.5\rho_0$, $\sim 2.75\rho_0$ and $\sim 3.1\rho_0$ for M_{DU} values of 1.6, 1.8, and 2.0 M_\odot , respectively. As expected, the highest values of M_{DU} correspond to the greatest values of ρ_{DU} , as shown in Table III. Since the symmetry energy at saturation remains constant for both families, it is the parameter L that governs the onset of DU processes. A larger value of L results in a lower onset density, as a larger L facilitates faster growth of symmetry energy beyond the saturation density.

B. Symmetry energy and Mass-Radius

The mass-radius relationship of a static NS can be determined by solving the Tolman-Oppenheimer-Volkoff (TOV) equation [65, 66], which incorporates the equation of state (EOS) of the NS, representing pressure as a function of energy density. We have included the Baym-Pethick-Sutherland outer crust [67], and the inner crust was treated as in [33]: the outer crust is matched to the outer core EoS at 0.04fm^{-3} using a polytrope. The matching density was chosen in order to reduce the error introduced, which was shown to be below 100 m [68]. Table III provides details on the maximum gravitational mass, its baryonic mass and radius, the mass M_{DU} and its central density ρ_{DU} , as well as the radius and central density of stars with masses of 1.6, 1.8, and 2.0 M_\odot . While the properties of the maximum mass star remain largely unchanged with the modifications introduced in the isovector channel, there is a noticeable impact on the radius, central density, DU mass and radius of stars with masses less than or equal to 2.0 M_\odot . Specifically, a larger slope L results in smaller M_{DU} and density ρ_{DU} , leading to reduced NS radii and central densities.

In Fig.4, we plot the mass-radius relation ($M - R$) for the modified DD2 and DDMEX models. Also included are some recent astrophysical observations (see the caption for details). As referred before, it is clearly seen that the maximum masses of NSs calculated using DD2 and DDMEX models are not very sensitive to the isovector channel, suffering a small increase not larger than $0.02M_\odot$. Notably, the DDMEX models, also the generalized parametrizations, demonstrate the capability to predict NSs exceeding $2.5M_\odot$, consistent with the observed mass range of the secondary compact object in GW190814, reported as $2.50 - 2.67M_\odot$ (see [44]). It is clearly seen that the effect of y and new values of a_ρ that allow DU processes to occur inside NS is not negligible: the radius of medium and high mass stars is 150-300 m larger due the much stiffer symmetry energy. In this figure we have also included the results of a Bayesian

inference calculation that will be discussed below.

In addition to the constraints provided by observations of massive NSs such as PSR J1614-2230, PSR J034+0432, and PSR J0740+6620, recent measurements from NICER have simultaneously determined the mass and radius of a NS in the intermediate mass region, PSR J0030+0451. According to [69] its mass is $1.44^{+0.15}_{-0.14} M_{\odot}$ with a radius of $13.02^{+1.24}_{-1.06}$ km, while [70] reports a mass of $1.34^{+0.15}_{-0.16} M_{\odot}$ with a radius of $12.71^{+1.14}_{-1.19}$ km. Across various models, as verified in previous studies [64, 71, 72], it is noted that a larger slope corresponds to larger radii for NSs with masses less than or equal to $2.0 M_{\odot}$. Specifically, for $1.4 M_{\odot}$ stars, the radius increases from 13 km to 13.5 km.

C. The isovector channel: Bayesian inference

In the previous section we discussed the main properties of the DD2 and DDMEX families, keeping fixed the isoscalar channel describing the symmetric nuclear matter EOS and the symmetry energy at saturation: the variation of the parameters y and a_{ρ} has allowed to vary the slope and the curvature of the symmetry energy at saturation. As discussed, a direct consequence was the effect these two parameters have on the onset of the nucleonic DU processes, allowing a decrease in the onset density and consequently a decrease in the mass of the NS with a central density coinciding with the DU onset density.

In the following we present a Bayesian analysis to constrain the complete isovector channel, i.e. the couplings $\Gamma_{\rho}(\rho_0)$, a_{ρ} and y , considering as constraints the onset of nucleonic DU and the low density chEFT neutron matter pressure. The corner plot shown in Fig. 5 summarises the main results: The bidimensional distributions relate the isovector channel parameters to the isovector nuclear matter properties $J_{\text{sym},0} \equiv E_{\text{sym},0}$, L_0 , $K_{\text{sym},0}$, and to the NS properties maximum mass M_{max} , radius for $1.4 M_{\odot}$ NS $R_{1.4}$, onset density of the DU processes ρ_{DU} and corresponding NS mass with this density at the centre M_{DU} . The two models previously discussed, DD2 and DDMEX, were considered as a starting point, in particular keeping all the parameters defining the isoscalar channel fixed. The results for the two models are shown in different colours, pink-red for DD2 and light-blue for DDMEX.

The main conclusions that can be drawn are: 1) the parameter y correlates not only with the onset density of DU, and corresponding mass, but also with the maximum star mass. The smaller y the smaller the onset density of DU and the larger the maximum star mass. Considering the constraints imposed it was not possible to get values for the mass M_{DU} below $\sim 2 M_{\odot}$ for the DDMEX family, but it is possible to go down to $\sim 1.6 M_{\odot}$ for the DD2 family at 99% CI. The parameter y also affects the properties L_0 , $K_{\text{sym},0}$, in particular, a smaller value of y pushes these two quantities to larger values; 2) a_{ρ} correlates strongly with the curvature $K_{\text{sym},0}$, giving larger

values, that can even be positive, for larger values of a_{ρ} . $K_{\text{sym},0}$ is in average larger for the DDMEX family, and at 68% CI it can take values of the order $\sim +30$ MeV. The largest values of M_{max} occur for the largest values of a_{ρ} ; 3) there is a clear correlation between L_0 and $R_{1.4}$ as shown in other studies when the isoscalar channel is kept fixed [64, 71, 72, 74]. Notice, however, that if the isoscalar channel is also allowed to vary this correlation seems to disappear [75, 76]. For both models chEFT constraints impose $40 \lesssim L_0 \lesssim 60$ MeV; 4) The coupling Γ_{ρ_0} , is totally correlated with $E_{\text{sym},0}$ by definition, and also correlated with $K_{\text{sym},0}$ the smaller values of this properties being associated with the larger values of the coupling Γ_{ρ_0} ; 5) the isovector channel does not affect much the NS maximum mass, a maximum variation of $0.1 M_{\odot}$ is obtained. It is also observed that the DDMEX family predicts masses $\sim 0.2 M_{\odot}$ larger than the DD2 family; 6) finally let us also point down the behavior of the families concerning the radius of the $1.4 M_{\odot}$, $R_{1.4}$: in average DD2 predicts radii ~ 400 m smaller than DDMEX family; 7) notice that no clear correlation between L_0 and $K_{\text{sym},0}$ is obtained, as discussed in the previous sections.

The comparison of the above results for the NS properties with the previous discussion allows some interesting conclusions: the prediction of the M_{DU} obtained are compatible with the values calculated in Table III, the lowest M_{DU} obtained was $1.6 M_{\odot}$ for the DD2 family with a slope L_0 greater than 60 MeV with 68% CI and $K_{\text{sym},0}$ slightly lower than 0, see DD2-1.6a, DD2-1.6b models in Tables II and III. The models DD2-1.8a, DD2-1.8b with a $M_{\text{DU}} = 1.8 M_{\odot}$ have a slope below 60 MeV. For DD2-2b, DD2-2c with $M_{\text{DU}} = 2.0 M_{\odot}$ with a slope around 55 MeV (for $y > 0.4$, a_{ρ} around 1.0) and a negative value of $K_{\text{sym},0} \lesssim 0$ and the density ρ_{DU} is between 0.37 fm^{-3} and 0.48 fm^{-3} . Note, however, that DD2-2a has a slope above 60 MeV because y takes a value above 0.5 contrary to all the other DD2 parametrizations. In summary, the smallest M_{DU} requires the largest values of L_0 and values of $K_{\text{sym},0}$ close to zero. However, large values of M_{DU} may also have large values of L_0 , but in this case the $K_{\text{sym},0}$ parameter is more negative: the larger L_0 the more negative $K_{\text{sym},0}$.

For reference we show the 90% CI distribution of the symmetry energy in Fig. 6. Also included, for comparison are the respective curves for DD2 and DDMEX. As expected, the DU constrain imposes a much harder symmetry energy at high densities.

In Fig. 4, the mass-radius 90% CI distribution resulting from the inference calculation is plotted for both DD2 and DDMEX families. These distributions have a large overlap for $M \lesssim 1.4 M_{\odot}$, because this is the region that is most affected by the chEFT constraints. Both models are compatible with the present observations due to the large uncertainties still associated with the measurements. Note that some of the parametrizations proposed in Table III lie outside the 90% credible level distributions because only extreme parametrizations could satisfy the conditions necessary to allow DU processes inside the NS.

TABLE III. The NS properties are given: the maximum mass M_{\max} and the DU mass M_{DU} , respective baryon mass $M_{B,\max}$ and radius R_{\max} , the radius of 1.4, 1.6, 1.8 and $2.0M_{\odot}$ stars, the DU onset baryon density ρ_{DU} and the central baryon density ρ_c .

Model	M_{\max}	M_{DU}	$M_{B,\max}$	R_{\max}	$R_{1.6}$	$R_{1.8}$	$R_{2.0}$	ρ_{DU}	ρ_c
	M_{\odot}								
DD2	2.42	–	2.92	11.87	13.22	13.21	13.20	–	0.852
DD2-1.6a	2.44	1.6	2.94	12.07	13.54	13.51	13.42	0.366	0.827
DD2-1.6b	2.44	1.6	2.94	12.06	13.50	13.48	13.40	0.37	0.828
DD2-1.8a	2.44	1.8	2.94	12.02	13.44	13.43	13.33	0.417	0.833
DD2-1.8b	2.44	1.8	2.94	12.02	13.40	13.39	13.31	0.415	0.832
DD2-2a	2.43	2.0	2.93	11.99	13.42	13.40	13.31	0.466	0.838
DD2-2b	2.44	2.0	2.94	11.98	13.36	13.35	13.27	0.472	0.836
DD2-2c	2.44	2.0	2.94	11.97	13.28	13.28	13.22	0.464	0.834
DDMEX	2.56	–	3.11	12.35	13.46	13.51	13.53	–	0.776
DDMEX-1.6	2.58	1.6	3.13	12.56	13.87	13.90	13.87	0.343	0.756
DDMEX-1.8a	2.58	1.8	3.13	12.53	13.80	13.84	13.83	0.366	0.758
DDMEX-1.8b	2.58	1.8	3.13	12.54	13.81	13.86	13.83	0.357	0.758
DDMEX-2a	2.57	2.0	3.12	12.49	13.76	13.80	13.78	0.40	0.763
DDMEX-2b	2.57	2.0	3.12	12.49	13.74	13.78	13.77	0.397	0.763
DDMEX-2c	2.57	2.0	3.13	12.47	13.67	13.73	13.72	0.403	0.763

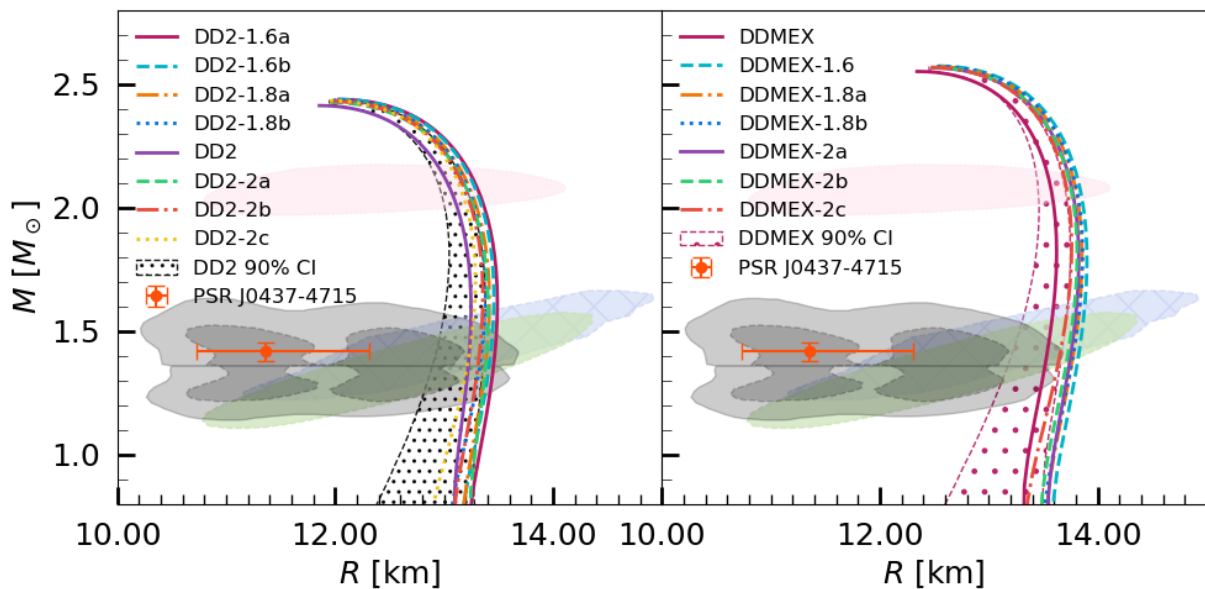


FIG. 4. Neutrons star masses versus the radius for the two DD families: left panel DD2 set, right panel DDMEX set. NS masses as a function of radius for the DD2 (blue) and DDMEX (orange) families, allowing the three couplings that define the isovector channel to vary, i.e. $\Gamma_{\rho}(\rho_0)$, a_{ρ} , y . Both the median and the 90% CI probability regions are plotted. The LIGO-Virgo collaboration and NICER observations are also shown: The grey lines represent the constraints derived from the binary components of GW170817, along with their corresponding 90% and 50% CI [3]. Also shown are the 1σ (68%) CI for the 2D posterior distribution in the mass-radius domain for the millisecond pulsars PSR J0030 + 0451 (cyan and violet) [69, 70] and PSR J0740 + 6620 (purple and peach) [5, 73] from the NICER X-ray data.

IV. CONCLUSION

In order to study the properties of NSs, in this paper, we considered two families of density-dependent relativistic mean-field models with stiff EOS, namely the DD2 and DDMEX families. These models are able to generate

NSs with masses as large as $2.44 M_{\odot}$ (DD2) and $2.57 M_{\odot}$ (DDMEX). In particular, DDMEX was constrained by the low mass compact object in the event GW190814, with a mass of $2.50\text{-}2.67 M_{\odot}$ [44]. A common behaviour of many DD models is that they do not predict the nucleonic DU processes inside nucleonic NSs ([26, 27]), due

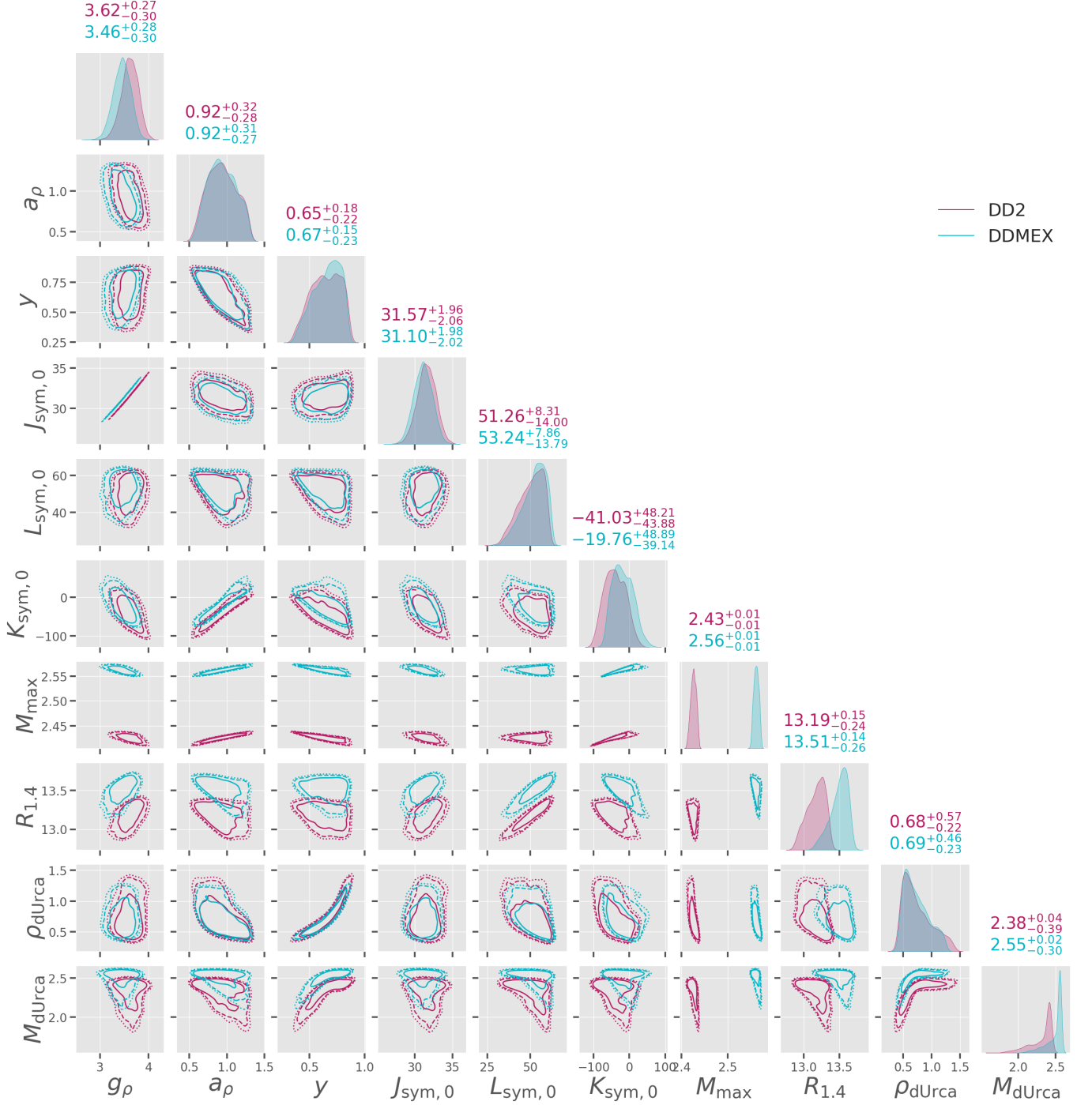


FIG. 5. Corner plot obtained by varying the parameters responsible for the isovector channel, Γ_{ρ_0} , a_ρ and y , using the parameterisation of DD2 (pink-red) and DDmEX (light-blue) for the isoscalar channel. Isovector nuclear matter properties ($J_{\text{sym},0} \equiv E_{\text{sym},0}$, $L_{\text{sym},0} \equiv L_0$, $K_{\text{sym},0}$) and NS properties (the maximum mass M_{max} , the radius for $1.4 M_\odot$ NS $R_{1.4}$, the onset density of the DU processes ρ_{DU} and the corresponding NS mass with this density at the center M_{DU}) are shown. The different line styles in the two-dimensional distribution (solid, dashed and dotted) correspond to 68%, 95% and 99% CI.

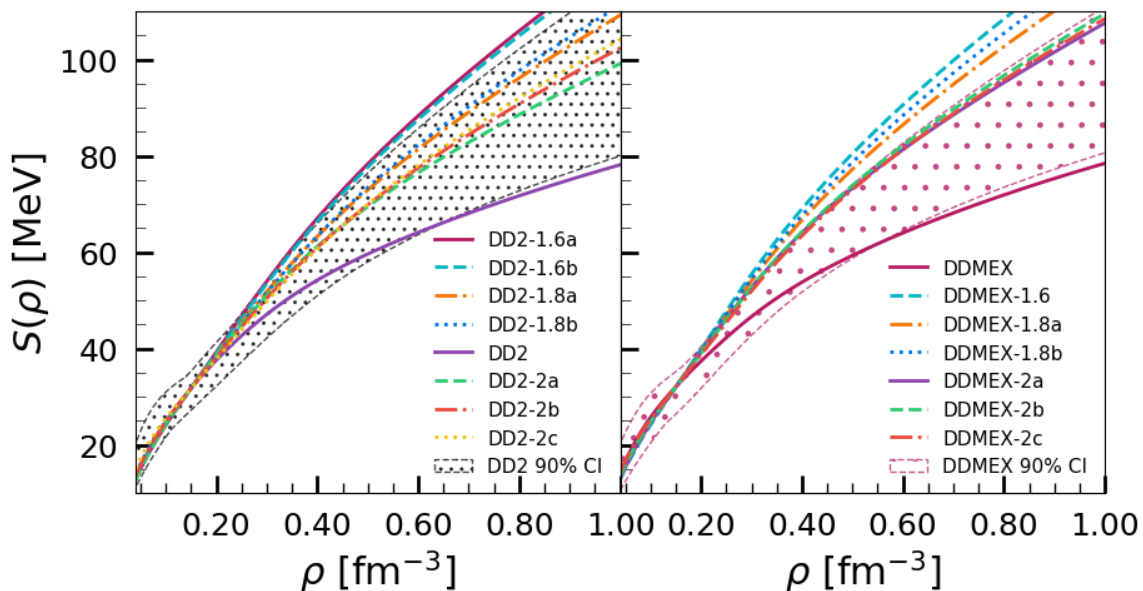


FIG. 6. The symmetry energy, denoted as $S(\rho) \equiv E_{\text{sym}}(\rho_B)$, is plotted against the number density ρ . Both $S(\rho)$ and ρ are measured in MeV and fm^{-3} respectively, across various isovector variations of the DD2 and DDMEX models. The median curve is depicted together with the 90% confidence interval.

to the exponential decrease of the ρ -meson coupling with density. To explain the cooling curves of the thermal evolution of isolated non-magnetized and non-rotating NSs or accreting NSs with these models, [27, 29] found it necessary to include hyperons inside the star. This may have the consequence of making the EOS too soft, and therefore not allowing for the existence of $2M_{\odot}$ mass stars, if the hadronic EOS is soft.

To overcome this limitation, we adopt a different approach and introduce a generalization of the ρ -meson coupling constrained by observations of NS cooling as shown in [37], allowing for the nucleonic DU processes to occur inside NS. The objective of the present work was to investigate the consequence of this new parameter on the nuclear matter properties and NS properties.

By adopting as a high-density constraint, the prediction of nucleonic DU processes inside NS, we have generated a set of DD models that obey the χ EFT EOS neutron matter constraints and satisfy nuclear matter saturation properties, namely saturation density, binding energy per particle, incompressibility and symmetry energy, according to the presently accepted values. For the isospin channel at low densities, we have considered an interval compatible with χ EFT calculations. In addition, the symmetry energy of the models was also constrained in order to produce a maximum star mass of at least $2M_{\odot}$. Notice, however, that the isospin channel does not have a large influence on the maximum mass and we did not obtain deviation larger than $0.1M_{\odot}$ from the original maximum masses predicted by DD2 and DDMEX.

The models we obtained allowed us to predict an onset of DU cooling processes inside stars with a mass $\gtrsim 1.6M_{\odot}$ ($\gtrsim 1.8M_{\odot}$) for the DD2 (DDMEX) family with maxi-

um masses and radii slightly larger than the maximum M-R of the original DD models ($2.42M_{\odot}$ for DD2 and $2.56M_{\odot}$ for DDMEX) and could still be compatible with the low-mass object of the binary merger at the origin of GW190814, $2.50\text{-}2.67M_{\odot}$ [77]. We note that considering the isoscalar channels of the models DD2 and DDMEX, the chEFT constraints excludes the appearance of the DU processes inside NS of masses below $1.6M_{\odot}$. Within these models, if stars with masses below $1.6M_{\odot}$ show a fast cooling it will be necessary to include hyperons, which could be envisaged in future work.

We have shown that to decrease the M_{DU} , it is necessary to increase L_0 . A direct consequence on the NS properties of increasing L_0 keeping the properties of the isoscalar channel fixed is the increase of the NS radius, the smaller the mass the larger the effect. At the maximum mass the effect was small but there was a clear reduction of the central density ρ_c .

It was shown that in order to allow for DU nucleonic processes inside NS described by these two families of EOS, $K_{\text{sym},0}$ may take values close to zero or positive.

In the literature it was often pointed out a correlation between L_0 and $K_{\text{sym},0}$ [59–61]. However, for the modified DD EOS verifying the high density constraints imposed by the DU process, the correlation L_0 - $K_{\text{sym},0}$ is washed out for both families of EOS. It is interesting to understand which are the effects on the low density region, below the saturation density, of considering the L_0 - $K_{\text{sym},0}$ coefficients determined from the high density constraints. These affect the densities that define the crust of the NS. More specifically, we are interested in studying the impact of the high-density constrained DD models on the critical and crust-core transitions proper-

ties.

ACKNOWLEDGMENTS

This research received partial funding from national sources through FCT (Fundação para a Ciência e a Tecnologia, I.P, Portugal) for projects UIDB/04564/2020 and UIDP/04564/2020, iden-

tified by DOI 10.54499/UIDB/04564/2020 and 10.54499/UIDP/04564/2020, respectively, as well as for project 2022.06460.PTDC with DOI 10.54499/2022.06460.PTDC. The authors acknowledge the Laboratory for Advanced Computing at the University of Coimbra for providing HPC resources that have contributed to the research results reported within this paper, URL: <https://www.uc.pt/lca>.

-
- [1] B. P. Abbott, R. Abbott, T. D. Abbott, and *et al.* (LIGO Scientific Collaboration and Virgo Collaboration), *Phys. Rev. Lett.* **119**, 161101 (2017).
- [2] B. P. Abbott, R. Abbott, T. D. Abbott, and *et al.*, *The Astrophysical Journal Letters* **848**, L12 (2017).
- [3] B. P. Abbott, R. Abbott, T. D. Abbott, and *et al.* (The LIGO Scientific Collaboration and the Virgo Collaboration), *Phys. Rev. Lett.* **121**, 161101 (2018).
- [4] B. P. Abbott, R. Abbott, T. D. Abbott, and *et al.*, *The Astrophysical Journal Letters* **892**, L3 (2020).
- [5] M. C. Miller, F. K. Lamb, A. J. Dittmann, S. Bogdanov, Z. Arzoumanian, K. C. Gendreau, S. Guillot, W. C. G. Ho, J. M. Lattimer, M. Loewenstein, S. M. Morsink, P. S. Ray, M. T. Wolff, C. L. Baker, T. Cazeau, S. Manthripragada, C. B. Markwardt, T. Okajima, S. Pollard, I. Cognard, H. T. Cromartie, E. Fonseca, L. Guillemot, M. Kerr, A. Parthasarathy, T. T. Pennucci, S. Ransom, and I. Stairs, *The Astrophysical Journal Letters* **918**, L28 (2021).
- [6] E. Annala, T. Gorda, E. Katerini, A. Kurkela, J. Nättilä, V. Paschalidis, and A. Vuorinen, *Phys. Rev. X* **12**, 011058 (2022).
- [7] B. Biswas, *The Astrophysical Journal* **926**, 75 (2022).
- [8] J. M. Lattimer, *Annual Review of Nuclear and Particle Science* **62**, 485 (2012), <https://doi.org/10.1146/annurev-nucl-102711-095018>.
- [9] M. Oertel, M. Hempel, T. Klähn, and S. Typel, *Rev. Mod. Phys.* **89**, 015007 (2017).
- [10] L. Tolos and L. Fabbietti, *Progress in Particle and Nuclear Physics* **112**, 103770 (2020).
- [11] K. Hebeler, *Physics Reports* **890**, 1 (2021), three-nucleon forces: Implementation and applications to atomic nuclei and dense matter.
- [12] G. Raaijmakers, S. K. Greif, K. Hebeler, T. Hinderer, S. Nisanke, A. Schwenk, T. E. Riley, A. L. Watts, J. M. Lattimer, and W. C. G. Ho, *The Astrophysical Journal Letters* **918**, L29 (2021).
- [13] J. J. Li, A. Sedrakian, and M. Alford, *Phys. Rev. D* **104**, L121302 (2021).
- [14] I. Legred, K. Chatziioannou, R. Essick, S. Han, and P. Landry, *Phys. Rev. D* **104**, 063003 (2021).
- [15] P. T. H. Pang, I. Tews, M. W. Coughlin, M. Bulla, C. V. D. Broeck, and T. Dietrich, *The Astrophysical Journal* **922**, 14 (2021).
- [16] S.-P. Tang, J.-L. Jiang, M.-Z. Han, Y.-Z. Fan, and D.-M. Wei, *Phys. Rev. D* **104**, 063032 (2021).
- [17] K. Hebeler, J. M. Lattimer, C. J. Pethick, and A. Schwenk, *The Astrophysical Journal* **773**, 11 (2013).
- [18] F. Weber, R. Negreiros, P. Rosenfield, and M. Stejner, *Progress in Particle and Nuclear Physics* **59** (2007), 10.1016/j.ppnp.2006.12.008.
- [19] M. G. Alford, S. Han, and K. Schwenzer, *Journal of Physics G: Nuclear and Particle Physics* **46**, 114001 (2019).
- [20] A. A.-C. D. G. H. Blaschke, D.; Ayriyan, *Universe Special Issue Compact Stars in the QCD Phase Diagram and in the Multi-Messenger Era of Astronomy* **6**, 81 (2020).
- [21] A. V. G. V. Bao-An Li, Ramos, *The European Physical Journal A* **50** (2014), <https://doi.org/10.1140/epja/i2014-14009-x>.
- [22] B.-J. Cai and B.-A. Li, *Phys. Rev. C* **103**, 054611 (2021).
- [23] A. Taninah, S. Agbemava, A. Afanasjev, and P. Ring, *Physics Letters B* **800**, 135065 (2020).
- [24] B. Wei, Q. Zhao, Z.-H. Wang, J. Geng, B.-Y. Sun, Y.-F. Niu, and W.-H. Long, *Chinese Physics C* **44**, 074107 (2020).
- [25] R. Brockmann and H. Toki, *Phys. Rev. Lett.* **68**, 3408 (1992).
- [26] M. Fortin, C. Providencia, A. R. Raduta, F. Gulminelli, J. L. Zdunik, P. Haensel, and M. Bejger, *Phys. Rev. C* **94**, 035804 (2016), arXiv:1604.01944 [astro-ph.SR].
- [27] M. Fortin, A. R. Raduta, S. Avancini, and C. Providência, *Phys. Rev. D* **103**, 083004 (2021), arXiv:2102.07565 [nucl-th].
- [28] M. V. Beznogov and D. G. Yakovlev, *Mon. Not. Roy. Astron. Soc.* **452**, 540 (2015), arXiv:1507.04206 [astro-ph.SR].
- [29] C. Providência, M. Fortin, H. Pais, and A. Rabhi, (2018), 10.3389/fspas.2019.00013, arXiv:1811.00786 [astro-ph.HE].
- [30] Y. Lim, A. Bhattacharya, J. W. Holt, and D. Pati, *Phys. Rev. C* **104**, L032802 (2021).
- [31] S. M. A. Imam, N. K. Patra, C. Mondal, T. Malik, and B. K. Agrawal, *Phys. Rev. C* **105**, 015806 (2022).
- [32] C. Mondal and F. Gulminelli, *Phys. Rev. D* **105**, 083016 (2022).
- [33] T. Malik, M. Ferreira, B. K. Agrawal, and C. ca Providência, *The Astrophysical Journal* **930**, 17 (2022).
- [34] K. Hebeler, J. M. Lattimer, C. J. Pethick, and A. Schwenk, *Astrophys. J.* **773**, 11 (2013), arXiv:1303.4662 [astro-ph.SR].
- [35] R. Essick, I. Tews, P. Landry, and A. Schwenk, *Phys. Rev. Lett.* **127**, 192701 (2021).
- [36] P. B. de Tovar, M. Ferreira, and C. c. Providência, *Phys. Rev. D* **104**, 123036 (2021).
- [37] T. Malik, B. K. Agrawal, and C. m. c. Providência, *Phys. Rev. C* **106**, L042801 (2022).
- [38] L. Scurto, H. Pais, and F. Gulminelli, *Phys. Rev. D* **109**, 103015 (2024), arXiv:2402.15548 [nucl-th].

- [39] B.-A. Li, B.-J. Cai, W.-J. Xie, and N.-B. Zhang, *Universe* **7**, 182 (2021), arXiv:2105.04629 [nucl-th].
- [40] M. Oertel, M. Hempel, T. Klähn, and S. Typel, *Rev. Mod. Phys.* **89**, 015007 (2017), arXiv:1610.03361 [astro-ph.HE].
- [41] B.-A. Li and X. Han, *Phys. Lett. B* **727**, 276 (2013), arXiv:1304.3368 [nucl-th].
- [42] J. M. Lattimer and Y. Lim, *Astrophys. J.* **771**, 51 (2013), arXiv:1203.4286 [nucl-th].
- [43] S. Typel, G. Röpke, T. Klähn, D. Blaschke, and H. H. Wolter, *Phys. Rev. C* **81**, 015803 (2010).
- [44] K. Huang, J. Hu, Y. Zhang, and H. Shen, *Astrophys. J.* **904**, 39 (2020), arXiv:2008.04491 [nucl-th].
- [45] S. Typel and D. A. Terrero, *The European Physical Journal A* **56**, 160 (2020).
- [46] G. A. Lalazissis, T. Nikisic, D. Vretenar, and P. Ring, *Phys. Rev. C* **71**, 024312 (2005).
- [47] S. Antić and S. Typel, *Nuclear Physics A* **938**, 92 (2015).
- [48] R. N. Mishra, H. S. Sahoo, P. K. Panda, N. Barik, and T. Frederico, *Phys. Rev. C* **92**, 045203 (2015).
- [49] T. Li, U. Garg, Y. Liu, R. Marks, B. Nayak, P. M. Rao, M. Fujiwara, H. Hashimoto, K. Kawase, K. Nakanishi, et al., *Physical review letters* **99**, 162503 (2007).
- [50] L.-W. Chen, C. M. Ko, and B.-A. Li, *Phys. Rev. Lett.* **94**, 032701 (2005), arXiv:nucl-th/0407032.
- [51] B.-A. Li, L.-W. Chen, and C. M. Ko, *Phys. Rept.* **464**, 113 (2008), arXiv:0804.3580 [nucl-th].
- [52] M. Centelles, X. Roca-Maza, X. Vinas, and M. Warda, *Phys. Rev. Lett.* **102**, 122502 (2009), arXiv:0806.2886 [nucl-th].
- [53] C. Drischler, K. Hebeler, and A. Schwenk, *Phys. Rev. C* **93**, 054314 (2016), arXiv:1510.06728 [nucl-th].
- [54] C. J. H. Brendan T. Reed, F. J. Fattoyev and J. Piekarewicz, (2023), arXiv:2305.19376v2 [Nuclear Theory (nucl-th)].
- [55] D. Adhikari et al. (PREX), *Phys. Rev. Lett.* **126**, 172502 (2021), arXiv:2102.10767 [nucl-ex].
- [56] D. Adhikari et al. (CREX), *Phys. Rev. Lett.* **129**, 042501 (2022), arXiv:2205.11593 [nucl-ex].
- [57] J. Margueron, R. Hoffmann Casali, and F. Gulminelli, *Phys. Rev. C* **97**, 025805 (2018), arXiv:1708.06894 [nucl-th].
- [58] C. Mondal, B. K. Agrawal, J. N. De, S. K. Samaddar, M. Centelles, and X. Viñas, *Phys. Rev. C* **96**, 021302 (2017), arXiv:1708.03846 [nucl-th].
- [59] Providência, Constança, Avancini, Sidney S., Cavnagnoli, Rafael, Chiacchiera, Silvia, Ducoin, Camille, Grill, Fabrizio, Margueron, Jérôme, Menezes, Débora P., Rabhi, Aziz, and Vidaña, Isaac, *Eur. Phys. J. A* **50**, 44 (2014).
- [60] C. Ducoin, J. Margueron, and C. Providência, *Europhysics Letters* **91**, 32001 (2010).
- [61] C. Ducoin, J. Margueron, C. Providência, and I. Vidaña, *Phys. Rev. C* **83**, 045810 (2011).
- [62] J. M. Lattimer, C. J. Pethick, M. Prakash, and P. Haensel, *Phys. Rev. Lett.* **66**, 2701 (1991).
- [63] T. Klähn, D. Blaschke, S. Typel, E. N. E. van Dalen, A. Faessler, C. Fuchs, T. Gaitanos, H. Grigorian, A. Ho, E. E. Kolomeitsev, M. C. Miller, G. Röpke, J. Trümper, D. N. Voskresensky, F. Weber, and H. H. Wolter, *Phys. Rev. C* **74**, 035802 (2006).
- [64] R. Cavagnoli, D. P. Menezes, and C. m. c. Providência, *Phys. Rev. C* **84**, 065810 (2011).
- [65] R. C. Tolman, *Phys. Rev.* **55**, 364 (1939).
- [66] J. R. Oppenheimer and G. M. Volkoff, *Phys. Rev.* **55**, 374 (1939).
- [67] G. Baym, C. Pethick, and P. Sutherland, *Astrophys. J.* **170**, 299 (1971).
- [68] T. Malik, H. Pais, and C. Providência, (2024), arXiv:2401.10842 [nucl-th].
- [69] M. C. Miller, F. K. Lamb, A. J. Dittmann, S. Bogdanov, Z. Arzoumanian, K. C. Gendreau, S. Guillot, A. K. Harding, W. C. G. Ho, J. M. Lattimer, R. M. Ludlam, S. Mahmoodifar, S. M. Morsink, P. S. Ray, T. E. Strohmayer, K. S. Wood, T. Enong, R. Foster, T. Okajima, G. Prigozhin, and Y. Soong, *The Astrophysical Journal Letters* **887**, L24 (2019).
- [70] T. E. Riley, A. L. Watts, S. Bogdanov, P. S. Ray, R. M. Ludlam, S. Guillot, Z. Arzoumanian, C. L. Baker, A. V. Bilous, D. Chakrabarty, K. C. Gendreau, A. K. Harding, W. C. G. Ho, J. M. Lattimer, S. M. Morsink, and T. E. Strohmayer, *The Astrophysical Journal Letters* **887**, L21 (2019).
- [71] J. Carriere, C. J. Horowitz, and J. Piekarewicz, *Astrophys. J.* **593**, 463 (2003), arXiv:nucl-th/0211015.
- [72] C. Providencia and A. Rabhi, *Phys. Rev. C* **87**, 055801 (2013), arXiv:1212.5911 [nucl-th].
- [73] T. E. Riley, A. L. Watts, P. S. Ray, S. Bogdanov, S. Guillot, S. M. Morsink, A. V. Bilous, Z. Arzoumanian, D. Choudhury, J. S. Deneva, K. C. Gendreau, A. K. Harding, W. C. G. Ho, J. M. Lattimer, M. Loewenstein, R. M. Ludlam, C. B. Markwardt, T. Okajima, C. Prescod-Weinstein, R. A. Remillard, M. T. Wolff, E. Fonseca, H. T. Cromartie, M. Kerr, T. T. Pennucci, A. Parthasarathy, S. Ransom, I. Stairs, L. Guillemot, and I. Cognard, *The Astrophysical Journal Letters* **918**, L27 (2021).
- [74] M. Salinas and J. Piekarewicz, *Phys. Rev. C* **107**, 045802 (2023), arXiv:2301.09692 [nucl-th].
- [75] N. Alam, B. K. Agrawal, M. Fortin, H. Pais, C. Providência, A. R. Raduta, and A. Sulaksono, *Phys. Rev. C* **94**, 052801 (2016), arXiv:1610.06344 [nucl-th].
- [76] P. Char, C. Mondal, F. Gulminelli, and M. Oertel, *Phys. Rev. D* **108**, 103045 (2023), arXiv:2307.12364 [nucl-th].
- [77] R. Abbott, T. D. Abbott, and *et al.*, *The Astrophysical Journal Letters* **896**, L44 (2020).